Operative Techniques in Otolaryngology 30 (2019) 171–179

Operative Techniques in
Otolaryngology

Radiological assessment of the vestibular system

Katherine L. Reinshagen, MD, Hugh D. Curtin, MD

From the Department of Radiology, Massachusetts Eye and Ear, Harvard Medical School, Boston, Massachusetts

KEYWORDS
Computed tomography;
Magnetic resonance imaging

Imaging is useful for the diagnosis, preoperative planning, and postoperative management for a number of vestibular pathologies. Computed tomography (CT) and magnetic resonance imaging (MRI) are the most commonly used modalities to assess the temporal bone. This review will discuss commonly used imaging techniques, review relevant anatomy on CT and MRI, and highlight examples of common vestibular pathologies on imaging.

Introduction

Imaging is helpful for diagnosis of vestibular pathology and can be useful for preoperative planning, and noninvasive monitoring of the postoperative patient for a number of vestibular pathologies. Computed tomography (CT) provides excellent bone detail, while magnetic resonance imaging (MRI) provides excellent soft tissue characterization. These modalities can often be complementary.

Computed tomography

Multidetector computed tomography provides fast, high spatial resolution images of the temporal bone. Because of the acquisition of thin section images, multiplanar reformats can easily be created directly on many Picture Archiving and Communication System (PACS) workstations, or alternatively, a dedicated 3D workstation often with third-party software. Reformatted images are particularly helpful in imaging of the temporal bone. Dedicated axial reformats parallel to the plane of the lateral semicircular canal, coronal images at 90° from the axial reformats, Stenvers (along the long axis of the petrous temporal bone), and Pöschl (perpendicular to the long axis of the petrous temporal bone) views provide different perspectives on the complex anatomy of the temporal bone.

Cone beam CT (CBCT) is another modality that can provide higher resolution images of the temporal bone. Because of the lengthier acquisition time, this modality is more prone to motion artifact. In addition, with the cone beam technique, each temporal bone is typically acquired separately. Some CBCT scanners have an architecture that only allows imaging in the sitting position making examination of children and some adults impossible. Soft tissues are not well characterized on CBCT because of its poorer soft tissue contrast discrimination compared to multidetector computed tomography.[1]

Magnetic resonance imaging

MRI is preferred for soft tissue characterization, definition of intracranial anatomy, and assessment of the fluid in the labyrinth. Imaging of the temporal bone can be done at 1.5 or 3 Tesla imaging and is typically acquired with high resolution (2-3 mm slice thickness), high matrix, small field of view imaging. A high resolution, cisterno-

Address reprint requests and correspondence: Katherine L. Reinshagen, MD, Department of Radiology, 243 Charles Street, Boston, MA 02114.
E-mail address: katherine_reinshagen@meei.harvard.edu

http://doi.org/10.1016/j.otot.2019.07.011
1043-1810/

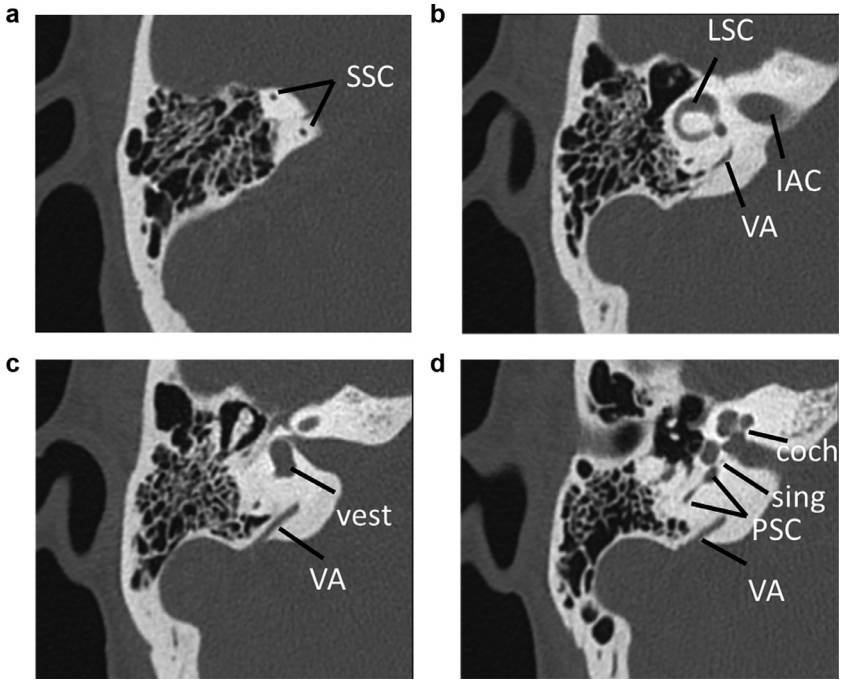

Figure 1 (a–d) Axial images from a normal temporal bone CT from superior to inferior. SSC, superior semicircular canal; LSC, lateral semicircular canal; VA, vestibular aqueduct; IAC, internal auditory canal; vest, vestibule; PSC, posterior semicircular canal; coch, cochlea; sing, singular nerve canal.

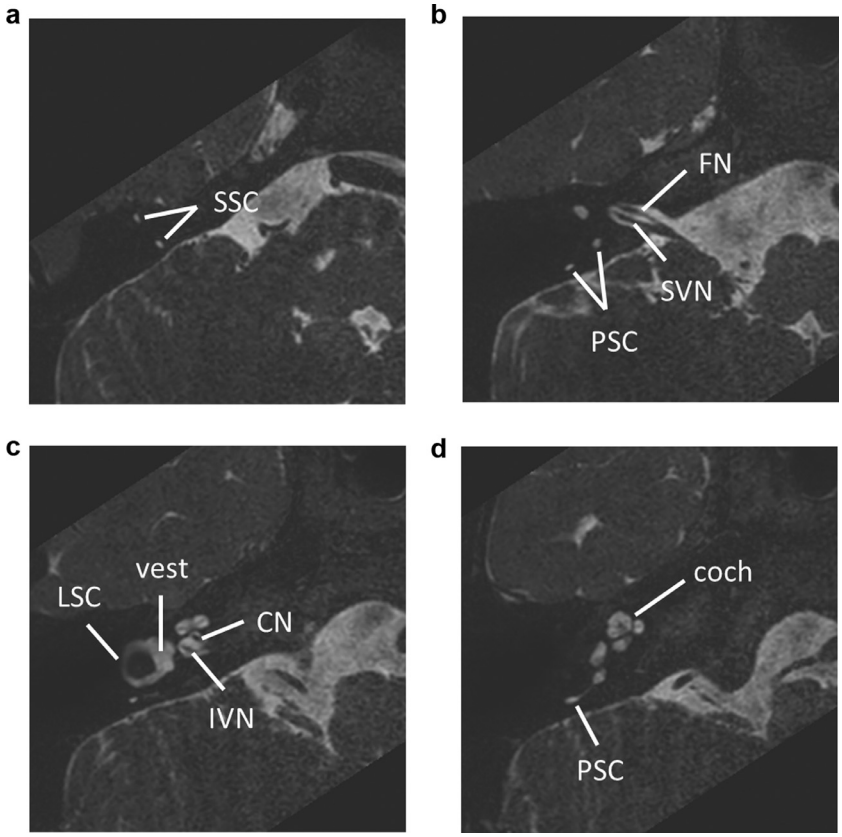

Figure 2 (a–d) Axial images from a normal temporal bone MR cisternographic sequence from superior to inferior. SSC, superior semicircular canal; PSC, posterior semicircular canal; SVN, superior vestibular nerve; FN, facial nerve; LSC, lateral semicircular canal; vest, vestibule; CN, cochlear nerve; IVN, inferior vestibular nerve; coch, cochlea.

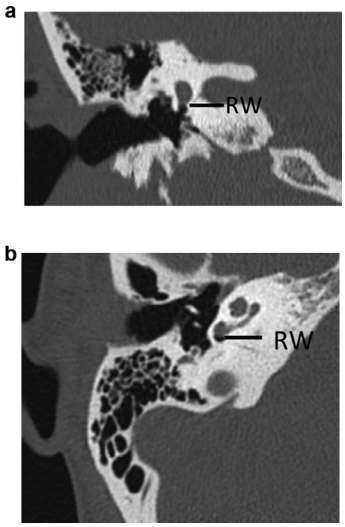

Figure 3 Coronal (a) and axial (b) CT images of a normal temporal bone demarcating the round window (RW).

graphic sequence (approximately 0.5 mm slice thickness) is particularly helpful for assessing the fluid in the vestibular and cochlear structures, as well as the intracanalicular and cisternal segments of the seventh and eighth cranial nerves. Intravenous gadolinium contrast can be helpful to assess for small tumors, as well as to assess for enhancement in the labyrinth, which can be seen in labyrinthitis. In addition to the cisternographic sequence, postsurgical imaging may also require fat-suppressed images as well as intravenous contrast to better differentiate between the bright signal of an enhancing tumor and bright signal seen with fat packing.

Imaging of the vestibular system

Normal anatomy

The vestibular system can be assessed with a combination of CT and MRI modalities. The bony margins and integrity of the semicircular canals are readily assessed with CT (Figure 1a–d), while the fluid within the labyrinth is better assessed with MRI (Figure 2a–d).

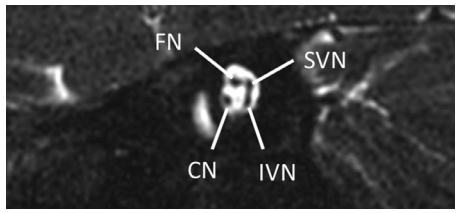

Figure 5 Reconstructed parasagittal view at the level of the internal auditory canal from a 3D volumetric cisternographic MR sequence demonstrating the location of the facial nerve (FN), cochlear nerve (CN), superior vestibular nerve (SVN), inferior vestibular nerve (IVN).

The bony margins of the vestibular aqueduct are better assessed with CT (Figure 1b–d), although pathology such as internal hemorrhage, proteinaceous fluid, or tumors along the endolymphatic sac and duct are better characterized by MRI.

The round window and vestibule can be readily seen with CT (Figure 3). The vestibule can also be readily identified on MR (Figure 2c). While the majority of the internal structure of the vestibule, including the saccule and the utricle, remain beyond the resolution of most clinical 3T MRI scanners, the macula of the utricle can often be seen with high-resolution cisternographic sequences (Figure 4).

The inferior and superior vestibular nerves, and the vestibulocochlear nerve can be visualized with a cisternographic MR sequence (Figures 2b,c and 5). While direct parasagittal images can be helpful to assess the nerves in the plane of the internal auditory canal, the reformatted images from a volumetric 3D acquisition is often sufficient requiring no additional time for the patient in the MR.

Pathology of the vestibular system

Semicircular canal dehiscence

Semicircular canal dehiscence is evaluated with CT because of the thin section bony detail required for assessment of possible third window pathology. Most commonly, the third window is identified as a superior semicircular canal dehiscence. Multiplanar reformatted images,

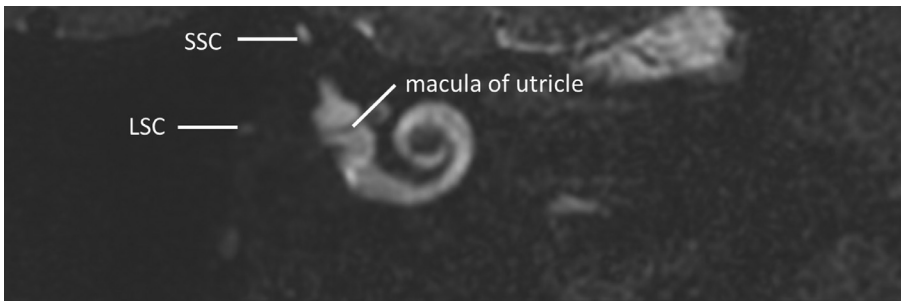

Figure 4 Reconstructed Stenvers view from a 3D volumetric cisternographic MR sequence demonstrating the macula of the utricle. SSC, superior semicircular canal; LSC, lateral semicircular canal.

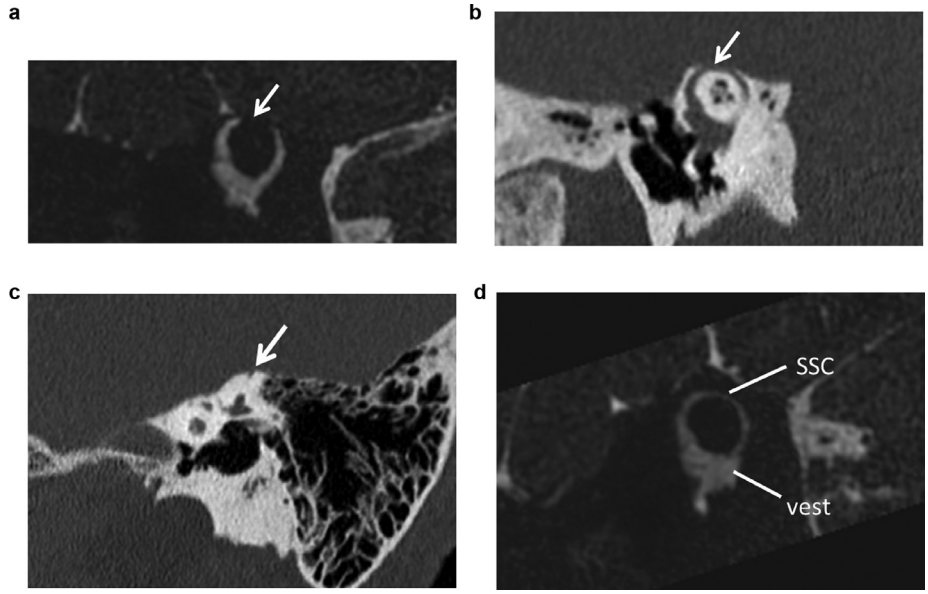

Figure 6 (a) Reconstructed Pöschl view from a 3D volumetric cisternographic MR sequence demonstrating the loss of fluid signal in the superior semicircular canal (arrow) status post middle cranial fossa approach repair with bone wax. (b) Reconstructed Pöschl and (c) Stenvers view from the postoperative CT demonstrates an apparent persistent defect along the superior semicircular canal (arrow) due to the presence of radiolucent bone wax. (d) Reconstructed Pöschl view from a 3D volumetric cisternographic MR sequence of the patient's normal contralateral superior semicircular canal (SSC), and vestibule (vest).

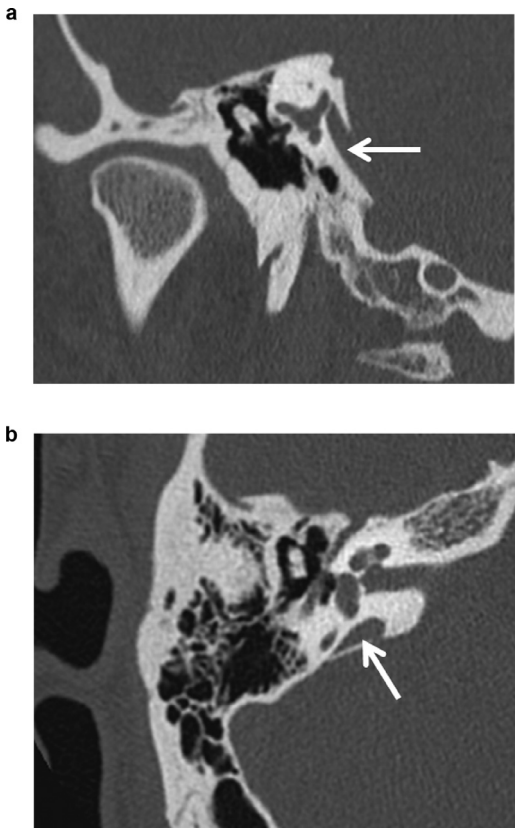

Figure 7 (a) Reconstructed Pöschl view from a temporal bone CT demonstrates an enlarged vestibular aqueduct (arrow). (b) Axial temporal bone CT demonstrates the oblique nature of the enlarged vestibular aqueduct (arrow).

particularly the Stenvers' plane (perpendicular to the superior semicircular canal) and Pöschl plane (parallel to the curve of the superior semicircular canal), allow for improved detection and characterization of small defects by demonstrating the superior semicircular canal in planes directly related to the canal. Other potential bony dehiscences along the other semicircular canals or even along the cochlear apex may potentially result in a third window phenomenon and are best appreciated with high-resolution CT.

Following treatment of superior semicircular canal dehiscence, MR may be helpful to confirm the absence of fluid signal in the superior semicircular canal to ensure adequate plugging.[2] MR is particularly helpful with the use of the nonradiopaque plugging materials, such as wax (Figure 6).

Meniere's disease

Currently, the role of imaging in suspected Meniere's disease is primarily to exclude other potential etiologies for the patient's symptoms of hearing loss and dizziness. Recent studies using off-label use of intratympanic gadolinium,[3,4] and 4-hour-delayed inversion recovery MR images following intravenous contrast are promising tools to assess the degree of endolymphatic hydrops and potentially follow patients during treatment.[5-9] However, 10%-33% of MD patients do not have changes on MR despite delayed postcontrast technique.[10-13] More investigation into these techniques is ongoing.

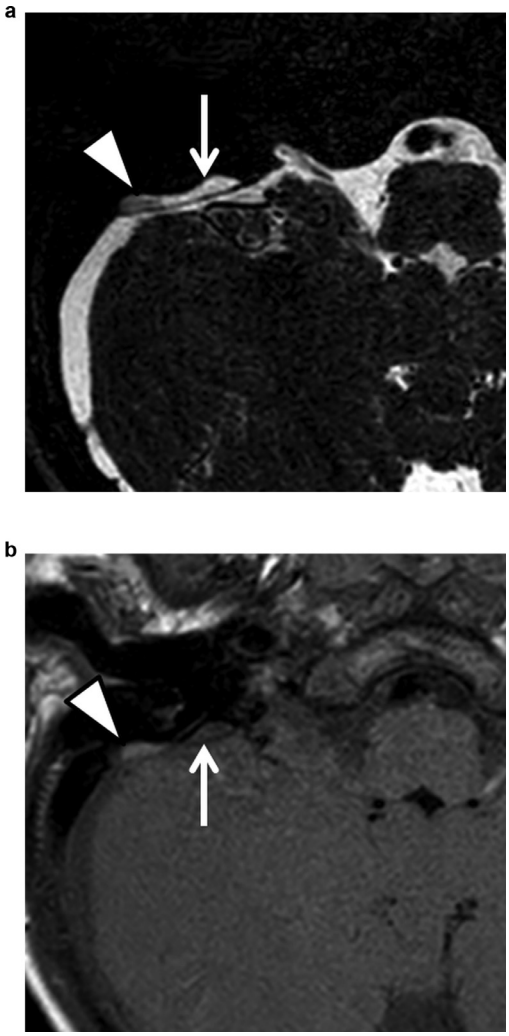

Figure 8 (a) Axial cisternographic MR sequence demonstrating an enlarged vestibular aqueduct with a distended endolymphatic sac (white arrow) with an area of decreased signal laterally (white arrowhead). (b) The noncontrast T1-weighted MR image at the same level shows the intrinsic T1 shortening (bright) signal corresponding to the area of decreased signal on the cisternographic sequence. Findings are consistent with hemorrhage or protein within the endolymphatic sac.

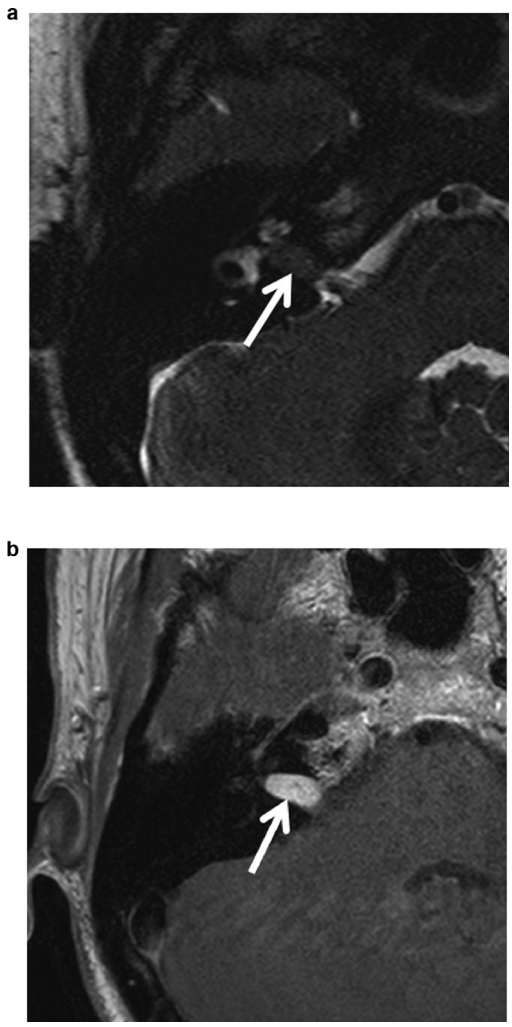

Figure 9 (a) Axial cisternographic MR sequence demonstrates a soft tissue lesion filling the right internal auditory canal and impacting the cochlear nerve aperture (arrow). (b) The lesion demonstrates avid enhancement on the postgadolinium T1-weighted image (arrow), consistent with a vestibular schwannoma.

Large vestibular aqueduct

The large vestibular aqueduct is classically assessed with CT imaging. Multiple radiographic criteria have been developed in an attempt to assess the size of the vestibular aqueduct. At our institution, we use the Pöschl plane (oblique 45° plane) as this plane is parallel to the long axis of the vestibular aqueduct, and thus not affected by the axial obliquity of the scan acquisition or obliquity of the vestibular aqueduct itself (Figure 7).[14] Based on a normal data set, a width of 0.8-0.9 mm at the midpoint of the vestibular aqueduct in the Pöschl plane is considered borderline to slightly enlarged.[15] The Cincinnati criteria uses the axial plane and defines the large vestibular aqueduct as greater than or equal to 2 mm at the level of the operculum, or greater than or equal to 1 mm at the midpoint.[16]

On MR, the large vestibular aqueduct is manifested by the presence of an enlarged fluid-filled endolymphatic sac and duct, which can be seen as a fluid-intensity oblique structure on the T2-weighted images. Occasionally, internal hemorrhage or proteinaceous fluid can be seen in the endolymphatic sac and may manifest as an area of heterogeneous signal intensity depending on the age of the hemorrhagic products or degree of proteinaceous material (Figure 8).

Intralabyrinthine and vestibular schwannomas

Schwannomas of the vestibular system are the most common neoplasm of the cerebellopontine angle. On MR, these commonly present as enhancing solid tumors (Figure 9). Approximately 10% of vestibular schwannomas demonstrate cystic change,[17,18] best appreciated on the T2-weighted sequences (Figure 10). The presence of a

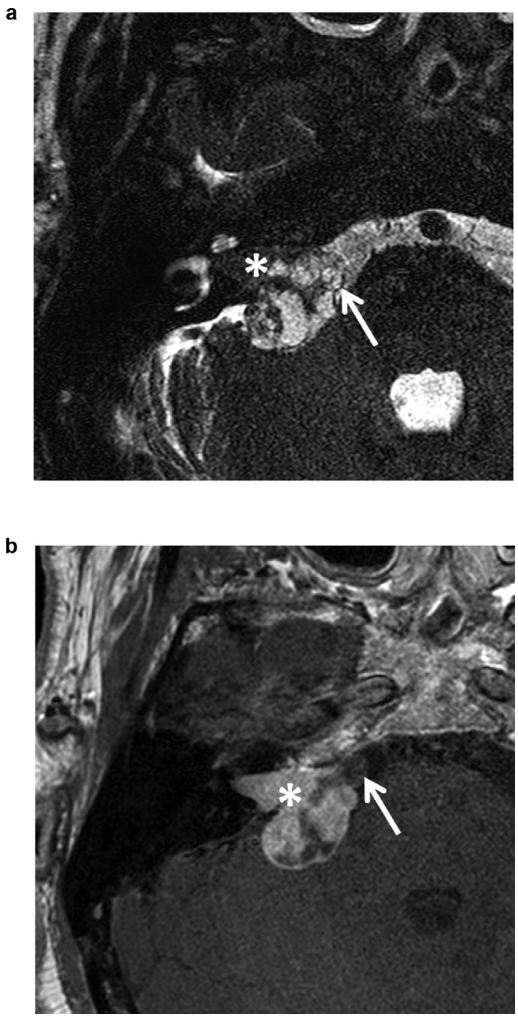

Figure 10 (a) Axial cisternographic MR sequence demonstrates a heterogeneous soft tissue lesion (asterisk) filling the right internal auditory canal, impacting the cochlear nerve aperture, and extending into the cerebellopontine angle cistern. There are areas of fluid signal intensity within the lesion (arrow). (b) The lesion demonstrates heterogeneous enhancement on the postgadolinium T1-weighted image (asterisk), and the internal areas of fluid signal do not demonstrate significant enhancement (arrow), suggesting cystic change within a vestibular schwannoma.

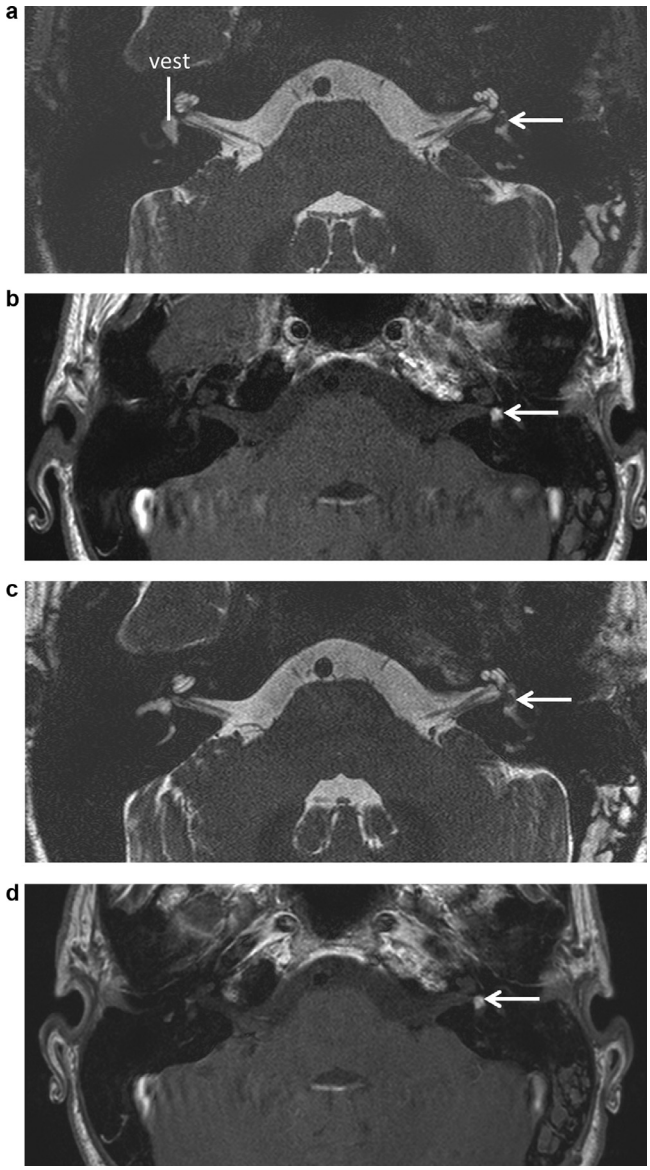

Figure 11 (a) Axial cisternographic MR sequence demonstrates a nodular filling defect within the left vestibule (arrow). The normal right vestibule (vest) is shown. (b) The left vestibular lesion demonstrates avid enhancement on the postgadolinium T1-weighted image (arrow). (c,d) The left vestibular lesion (arrow) is nearly identical 1 year later, suggesting an intralabyrinthine schwannoma as opposed to an inflammatory process.

vestibular schwannoma in the internal auditory canal may result in decreased T2 signal in the labyrinth, which has been hypothesized to reflect higher protein content in the labyrinthine fluid.[19] The lower signal is associated with decreased rates of hearing preservation after treatment.[20] On CT, small vestibular schwannomas are often impossible to see. Larger vestibular schwannomas may be suggested with smooth widening and expansion of the internal auditory canal and porous acousticus.

Intralabyrinthine schwannomas are rare occurring in just over 1 in 100,000 people in one study.[21] These are commonly seen as slow growing, enhancing tumors in the cochlea or vestibule (Figure 11). A lack of significant change in morphologic characteristics over time can be helpful in distinguishing an enhancing tumor from focal labyrinthitis.

Follow-up of vestibular schwannomas often does not require gadolinium contrast administration if the lesion is readily seen on high-resolution cisternographic sequences.[22] This should be considered in light of new evidence of gadolinium deposition in the brain following repeated contrast administration.[23]

Postsurgical imaging is often required to assess for residual tumor or tumor recurrence. Because of the frequent use of fat packing along the temporal bone, fat-suppressed T1-weighted postgadolinium images are often very helpful in the postoperative setting. Linear enhancement along the postsurgical site is an expected finding

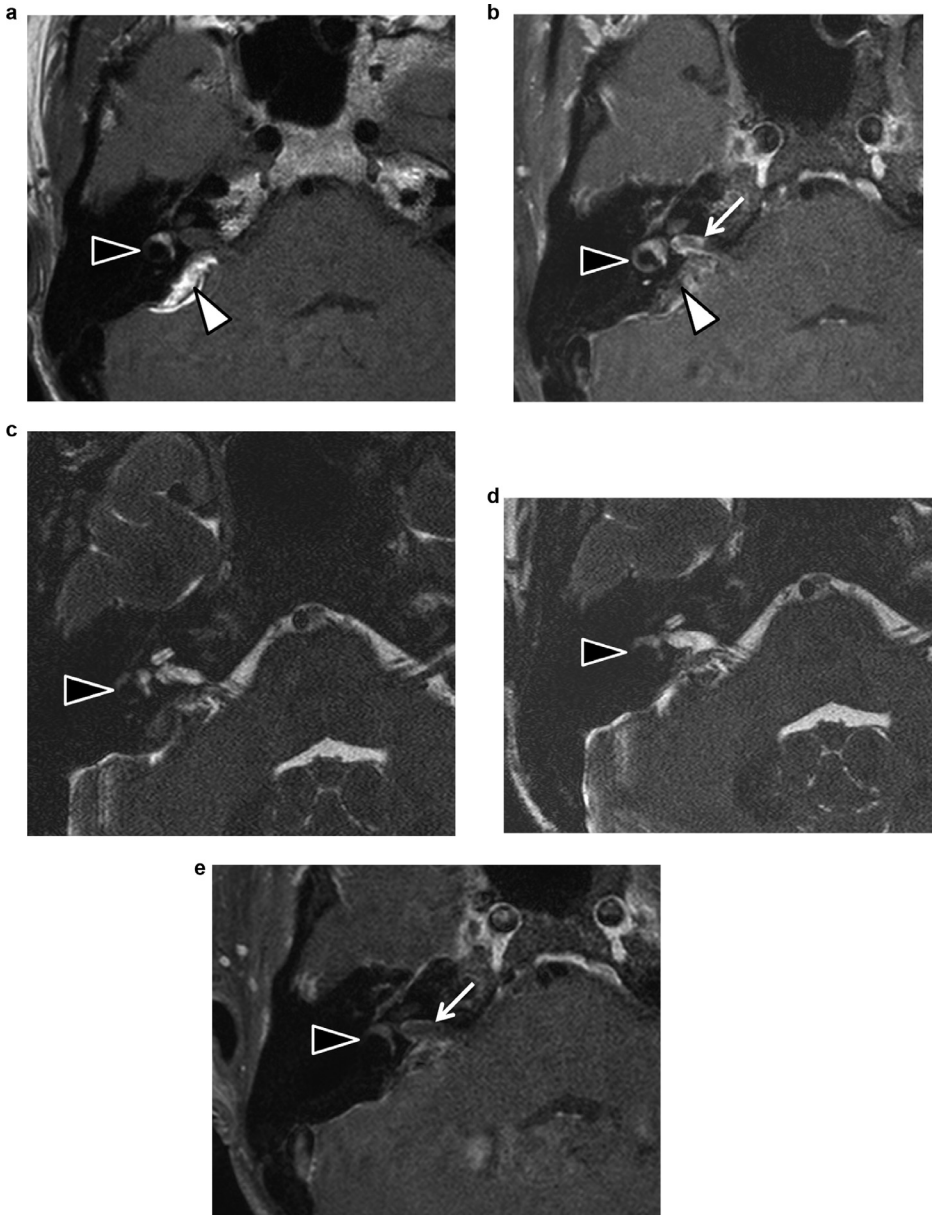

Figure 12 (a) Axial T1-weighted precontrast image of a patient immediately following resection of the right vestibular schwannoma. There is T1 shortening (bright signal) along the posterior right petrous ridge (white arrowhead), consistent with fat packing. There is no significant T1 shortening along the lateral semicircular canal (black arrowhead). (b) On the postcontrast fat-suppressed T1-weighted images, there is enhancement within the lateral semicircular canal (black arrowhead), linear enhancement along the right internal auditory canal (white arrow), and loss of the T1 shortening along the fat packing due to the fat suppression technique (white arrowhead). (c) Axial cisternographic MR sequence demonstrates loss of the normal fluid signal in the lateral semicircular canal. Findings are suggestive of early labyrinthitis within the lateral semicircular canal with expected postsurgical changes in the internal auditory canal. (d) In the same patient 4 years later, there is persistent loss of the fluid signal in the lateral semicircular canal (black arrowhead). (e) Four years later, on the postgadolinium fat-suppressed T1-weighted image, there is resolution of the enhancement within the lateral semicircular canal (black arrowhead), consistent with chronic labyrinthitis. There is also diminished linear enhancement in the internal auditory canal (white arrow), consistent with postoperative change. No nodular enhancing lesion was identified to suggest tumor recurrence.

likely relating to granulation or scar tissue (Figure 12). Nodular enhancement on the T1-weighted postgadolinium images should be viewed as suspicious for tumor recurrence (Figure 13).

Labyrinthitis ossificans

Labyrinthitis, an inflammatory condition involving the perilymphatic space, and secondarily involving the endolymphatic space, has various stages. The earliest imaging manifestation is best seen on MR as enhancement within the labyrinth seen on postcontrast T1-weighted im-

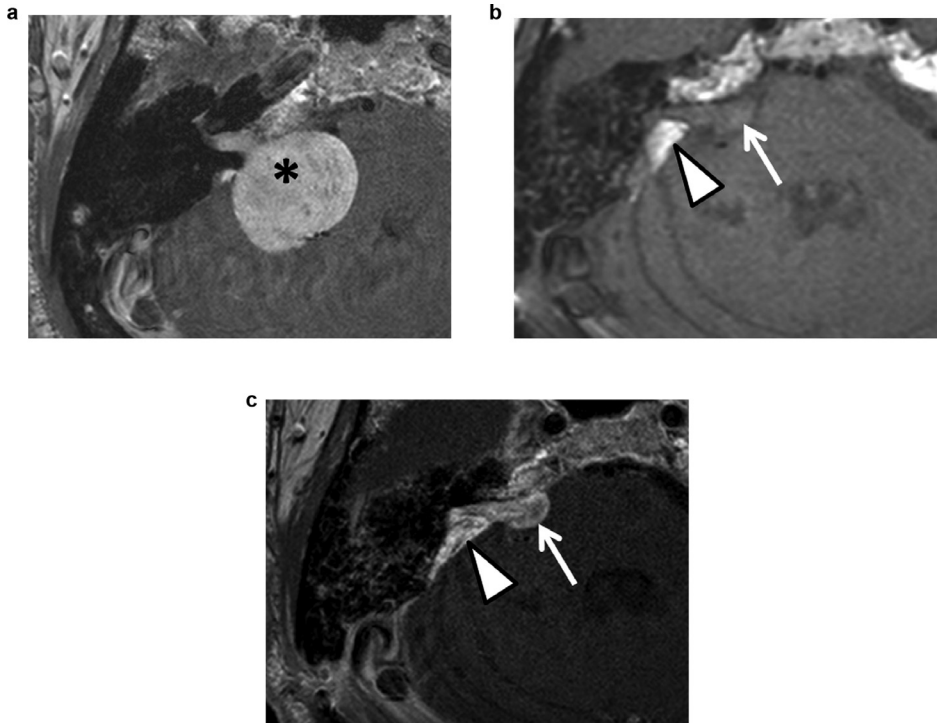

Figure 13 (a) Axial postgadolinium T1-weighted image demonstrates a large enhancing vestibular schwannoma (asterisk) extending into the cerebellopontine angle cistern with mass effect along the pons and middle cerebellar peduncle. (b) Postoperative T1-weighted and (c) postoperative postgadolinium T1-weighted image demonstrates residual enhancing soft tissue along the anterior margin of the right internal auditory canal extending into the cerebellopontine angle cistern (arrow), concerning for recurrent tumor. Fat packing is noted along the posterior margin of the right petrous ridge (white arrowhead).

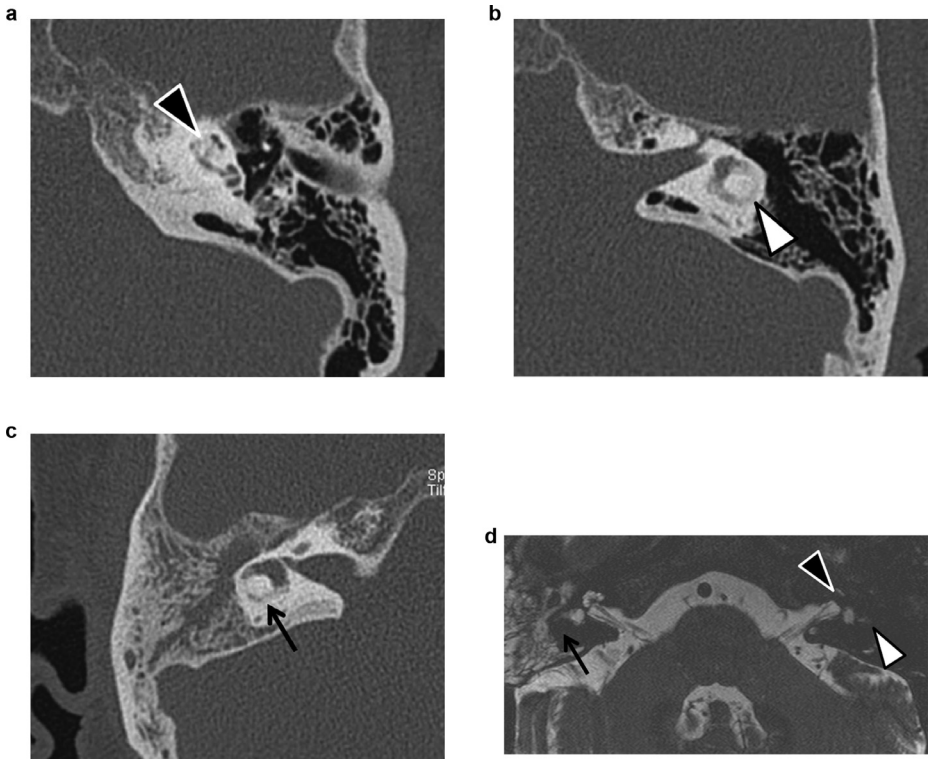

Figure 14 (a-c) Axial CT images demonstrate ossification of the left cochlea (black arrowhead), left lateral semicircular canal (white arrowhead), and the right lateral semicircular canal (black arrow). (d) Axial cisternographic MR sequence demonstrates loss of the fluid signal in the right lateral semicircular canal (black arrow), left cochlea (black arrowhead), and left lateral semicircular canal (white arrowhead). Findings consistent with the ossific stage of labyrinthitis.

ages. Loss of the fluid (T2 hyperintense) signal on heavily T2-weighted or cisternographic sequences with persistent enhancement suggests the fibrous stage of labyrinthitis (Figure 12).[24] During the acute and fibrous stage, CT will be negative. The ossific stage of labyrinthitis is best appreciated on CT (Figure 14). While there are many reasons for labyrinthitis including postmeningitis, viral disease, this is also a common postoperative finding (Figure 12).

Disclosure

Dr. Hugh Curtin receives royalties from Elsevier.

References

1. Miracle AC, Mukherji SK: Conebeam CT of the head and neck, part 1: Physical principles. AJNR Am J Neuroradiol 30:1088–1095, 2009.
2. Chemtob RA, Epprecht L, Reinshagen KL, et al: Utility of postoperative magnetic resonance imaging in patients who fail superior canal dehiscence surgery. Otol Neurotol 40(1):130–138, 2019.
3. Naganawa S, Sone M, Yamazaki M, et al: Visualization of endolymphatic hydrops after intratympanic injection of Gd-DTPA: Comparison of 2D and 3D real inversion recovery imaging. Magn Reson Med Sci 10:101–106, 2011.
4. Nakashima T, Naganawa S, Sugiura M, et al: Visualization of endolymphatic hydrops in patients with Meniere's disease. Laryngoscope 117:415–420, 2007.
5. Baráth K, Schuknecht B, Naldi AM, et al: Detection and grading of endolymphatic hydrops in Menière disease using MR imaging. AJNR Am J Neuroradiol 35:1387–1392, 2014.
6. Bernaerts A, De Foer B: Imaging of Ménière disease. Neuroimaging Clin N Am 29:19–28, 2019.
7. Naganawa S, Nakashima T: Visualization of endolymphatic hydrops with MR imaging in patients with Ménière's disease and related pathologies: Current status of its methods and clinical significance. Jpn J Radiol 32:191–204, 2014.
8. Lingam RK, Connor SEJ, Casselman JW, et al: MRI in otology: Applications in cholesteatoma and Ménière's disease. Clin Radiol 73:35–44, 2018.
9. Sepahdari AR, Vorasubin N, Ishiyama G, et al: Endolymphatic hydrops reversal following acetazolamide therapy: Demonstration with delayed intravenous contrast-enhanced 3D-FLAIR MRI. AJNR Am J Neuroradiol 37:151–154, 2016.
10. Pakdaman MN, Ishiyama G, Ishiyama A, et al: Blood-labyrinth barrier permeability in Menière disease and idiopathic sudden sensorineural hearing loss: Findings on delayed postcontrast 3D-FLAIR MRI. AJNR Am J Neuroradiol 37:1903–1908, 2016.
11. Sepahdari AR, Ishiyama G, Vorasubin N, et al: Delayed intravenous contrast-enhanced 3D FLAIR MRI in Meniere's disease: Correlation of quantitative measures of endolymphatic hydrops with hearing. Clin Imaging 39:26–31, 2015.
12. Seo YJ, Kim J, Choi JY, et al: Visualization of endolymphatic hydrops and correlation with audio-vestibular functional testing in patients with definite Meniere's disease. Auris Nasus Larynx 40:167–172, 2013.
13. Pyykkö I, Nakashima T, Yoshida T, et al: Meniere's disease: A reappraisal supported by a variable latency of symptoms and the MRI visualisation of endolymphatic hydrops. BMJ Open 3(2), 2013 PubMed.
14. Ozgen B, Cunnane ME, Caruso PA, et al: Comparison of 45 degrees oblique reformats with axial reformats in CT evaluation of the vestibular aqueduct. AJNR Am J Neuroradiol 29:30–34, 2008.
15. Juliano AF, Ting EY, Mingkwansook V, et al: Vestibular aqueduct measurements in the 45° oblique (Pöschl) plane. AJNR Am J Neuroradiol 37:1331–1337, 2016.
16. Boston M, Halsted M, Meinzen-Derr J, et al: The large vestibular aqueduct: A new definition based on audiologic and computed tomography correlation. Otolaryngol Head Neck Surg 136:972–977, 2007.
17. Piccirillo E, Wiet MR, Flanagan S, et al: Cystic vestibular schwannoma: Classification, management, and facial nerve outcomes. Otol Neurotol 30:826–834, 2009.
18. Lin EP, Crane BT: The management and imaging of vestibular schwannomas. AJNR Am J Neuroradiol 38:2034–2043, 2017.
19. O'Connor AF, France MW, Morrison AW: Perilymph total protein levels associated with cerebellopontine angle lesions. Am J Otol 2:193–195, 1981.
20. Somers T, Casselman J, de Ceulaer G, et al: Prognostic value of magnetic resonance imaging findings in hearing preservation surgery for vestibular schwannoma. Otol Neurotol 22:87–94, 2001.
21. Marinelli JP, Lohse CM, Carlson ML: Incidence of intralabyrinthine schwannoma: A population-based study within the United States. Otol Neurotol 39:1191–1194, 2018.
22. Buch K, Juliano A, Stankovic KM, et al: Noncontrast vestibular schwannoma surveillance imaging including an MR cisternographic sequence: Is there a need for postcontrast imaging? J Neurosurg 10:1–6, 2018 [Epub ahead of print].
23. McDonald RJ, McDonald JS, Kallmes DF, et al: Gadolinium deposition in human brain tissues after contrast-enhanced MR imaging in adult patients without intracranial abnormalities. Radiology 285:546–554, 2017.
24. Swartz JD, Hagiwara M. Inflammatory diseases of the temporal bone. In: Som PM, Curtin HD, editors. Head and Neck Imaging. ed 5 St. Louis: Mosby. 2011, p. 1218–1219.